J Mater Sci (2008) 43:2387–2392
DOI 10.1007/s10853-007-2028-5

Simulation of the adsorption of $CaCl_2$ on $Mg(OH)_2$ planes

Qi Wang · Lan Xiang · Ying Cai Zhang · Yong Jin

Received: 13 November 2006 / Accepted: 20 July 2007 / Published online: 22 December 2007

Abstract The adsorption behavior of Ca^{2+} and Cl^- on $Mg(OH)_2$ planes was simulated using Universal Force Field method. The energy, the capacity and the configuration involved in the adsorption process were estimated. The results showed that Ca^{2+} was easier to be adsorbed and incorporated on the (001) plane than other planes such as (100), (101) and (110) planes. The incorporation of Cl^- in $Mg(OH)_2$ was difficult since the radius for Cl^- is much bigger than that of OH^-. The adsorption of Ca^{2+} on (001) plane at elevated temperature may inhibit the growth along [001] direction, leading to occurrence of the (001) plane, the shrinkage of the (101) and (110) planes and the formation of $Mg(OH)_2$ plates with bigger ratios of diameter to thickness.

Introduction

The growth of crystal from solution is an important and interesting process. The morphology of the crystal was usually needed to be controlled in practice. Up to now many theoretical models (such as the BFDH [1], the PBC [2] and the interface-phase models [3]) have been developed to explore the influence of the inherent structure and the solution environment on the morphology of the crystal. It's known that the morphology of crystal was determined by the growth rates of the crystalline planes as well as the existence of the foreign substances. Many ions such as Cu^{2+}, Mg^{2+} [4], Fe^{2+}, Mg^{2+}, SO_4^{2-} [5], Na^+, Cl^- [6] can affect the growth rate and the morphology of the crystal. For example, the growth rate of calcite was reduced by the incorporation of Mg^{2+}, Cd^{2+} and Sr^{2+} [7]. Spherical calcite was produced in solution containing Mg^{2+} and SO_4^{2-} ions while rhombohedra calcite occurred in solution containing only Mg^{2+} or SO_4^{2-} [5].

The growth of $Mg(OH)_2$ crystal has attracted much attention in recent years since $Mg(OH)_2$ with different morphologies (needle-, plate- and rod-like shapes) can be used as functional powders in many fields such as electronics, catalyst, nano-composites and flame retardant [8–9]. The wet route (mixing of $MgCl_2$ and the alkaline (NaOH, NH_4OH or $Ca(OH)_2$) solutions at room temperature followed with the hydrothermal treatment) was one of the main methods to synthesis functional $Mg(OH)_2$ powders. The former studies [10–11] showed that the growth of $Mg(OH)_2$ was affected by the existence of the ions as Mg^{2+}, Ca^{2+}, SO_4^{2-} and OH^-. For example, Phillips found that the adsorption of Ca^{2+} on the (001) plane of $Mg(OH)_2$ led to the formation of $Mg(OH)_2$ plates with larger size [12].The growth of $Mg(OH)_2$ was influenced by the existence of OH^-: the increase of pH from 9 to 11 favored the growth of the platelets along edgewise, while the decrease of pH from 9 to 7 tended to decrease the ratio of the diameter to the thickness [13]. Henrist showed that the globular cauliflower-like and plate-like $Mg(OH)_2$ were formed in NaOH and NH_4OH solutions, separately, owing to the different structures of the cations [14]. However, most of the former works were mainly focused on the experimental observation of the growth phenomena and the detail growth mechanism was seldom reported.

Project supported by the National Natural Science Foundation of China (No. 50574051).

Q. Wang · L. Xiang (✉) · Y. C. Zhang · Y. Jin
Department of Chemical Engineering, Tsinghua University, Beijing, China
e-mail: xianglan@flotu.org

This paper investigated the influence of $CaCl_2$ on the hydrothermal modification of $Mg(OH)_2$ both experimentally and theoretically. The adsorption of Ca^{2+} and Cl^- on the hydrothermal growth and then on the morphology of $Mg(OH)_2$ crystal was simulated using the atomistic dynamics simulation method. The energy, the capacity and the configuration in the adsorption process were estimated and the mechanism involved in the hydrothermal modification of $Mg(OH)_2$ in $CaCl_2$ solution was discussed.

Experimental

200 mL of 2.0 mol/L NaOH was added into 200 mL of 4.0 mol/L $MgCl_2$. The suspension was stirred for 1.0 h and aged for 1.0 h at room temperature. After filtration and washing, the $Mg(OH)_2$ precipitate was mixed with $CaCl_2$ and re-dispersed ultrasonically in the deionized water to obtain a suspension containing 100 g/L of $Mg(OH)_2$ and 0–3 g/L of $CaCl_2$. 40 mL of the suspension was then placed in a polytetra fluoroethylen lined stainless steel autoclave with an inner volume of 80 cm^3. Then the autoclave was heated (5 °C/min) to 200 °C and kept stirring in isothermal condition for 4.0 h. After hydrothermal treatment, the suspension was filtered and dried in air at 105 °C for 12 h. The morphology of the particles was examined with a field scanning electron microscope (FSEM, Model JSM-6301, JEOL, Japan). The crystallinity of the sample was identified with the powder X-ray diffractometer (XRD, Model D/max-RB, Nigaku, Japan). The composition was analyzed by fluorescent-X ray spectroscope (Model XRF-1700, Shimadzu, Japan).

Theoretical simulation

Simulation technique

The computer code used for the atomistic dynamics simulation of Ca^{2+} and Cl^- on the $Mg(OH)_2$ planes was the Sorption package in Materials Studio software [15]. The $Mg(OH)_2$ unit cell was geometry optimized using Smart algorithm based on the principle of the minimum energy. The optimized $Mg(OH)_2$ unit cell was used to produce the planes and to build the framework. In the case of a fixed pressure and temperature, the sorbate can flow in or out of the framework to keep the pressure unchanged and the total energy of a configuration (m) is as follows:

$$E_m = E_m^{SS} + E_m^{SF} + U_m^S \tag{1}$$

where E_m^{SS} is the intermolecular energy between the sorbate; E_m^{SF} is the interaction energy between the sorbate and the framework, which is evaluated by the Ewald summation method; U_m^S is the total intramolecular energy of the sorbate, which is neglected when the sorbate is monatomic ion.

The probability of a configuration m in the grand canonical ensemble is given by [16]:

$$\rho_m = CF(\{N\}_m)\exp[-\beta E_m] \tag{2}$$

$$\beta = \frac{1}{K_B T} \tag{3}$$

where K_B is the Boltzmann constant, T is the absolute temperature, C is an arbitrary normalization constant, β is the reciprocal temperature, and E_m is the total energy of configuration m. The total absorption capacity for the components in configuration m is denoted by $\{N\}_m$. For a single component, the function $F(N)$ is given by:

$$F = \left(\frac{(\beta f V)^N}{N!}\right)\exp[-\beta N \mu_{\text{intra}}] \tag{4}$$

where F is the fugacity relating to the total potential energy of the sorbate, μ_{intra} is the intramolecular potential energy, and N is the adsorption capacity of the component.

The fixed pressure simulation starts with the empty framework. The starting configuration will take several steps to adjust to the specified fugacity and temperature. So the simulation is composed of two stages: the equilibrium and the production stages. The properties returned at the end of the run are based on the production stage only. Each step starts with the selection of a step type which could be the sorbate exchanges with the reservoir or a translation, rotation, or torsion change, depending on the Metropolis Monte Carlo method. This method is then used to decide whether to accept or reject the change.

The equilibrium morphology of $Mg(OH)_2$ was estimated using the Morphology package in the Material Studio software. The equilibrium morphology of a crystal is determined by the minimum surface energy for a given plane, which is proportional to the center-to-face distance. The equilibrium morphology of a crystal can be visualized using a Wulff plot if the surface energies for all of the crystal planes are known [17]. The surface energy of a plane is calculated as follows:

$$E_{surf} = \frac{1}{2}\lim_{M\to\infty}\frac{[E_{latt}(M) - E_{slice}(M)]}{A_{hkl}} \tag{5}$$

where $E_{latt}(M)$ and $E_{slice}(M)$ are the energy of a plane with M layer thickness in the crystal and in the vacuum, respectively, A_{hkl} is the surface area of a plane with Miller indices $\{h\ k\ l\}$. The factor 1/2 accounts for the fact that the slab has two surfaces.

Force field and parameters

The adsorption dynamic simulation is based on Universal Force Field which is a purely diagonal, harmonic forcefield developed by Rappe [18–19]. This energy expression describes the potential energy surface of a particular structure as a function of its atomic coordinates. The potential energy of the systerm can be expressed as a sum of bond and non-bond interactions.

$$E = E_{bond} + E_{nonbond} \tag{6}$$

The interaction energy in the forcefield is as follows: The energy of bond interaction is generally accounted for: Bond stretching (E_R) (8) is represented by the harmonic term, where k_{ij} is the force constants, r_{ij} is the bond length. Angle bending (E_θ) (9), torsions (E_ω) (10) and inversions (E_φ) (11) are represented by the Fourier cosine expansion, where k_{ijkl} is the force constants, C is the concordance factor, θ is the bend angle, ω is the angle torsions and φ is the angle inversions.

$$E_{bond} = E_R + E_\theta + E_\phi + E_\chi \tag{7}$$

$$E_R = 1/[2k_{ij}(r - r_{ij})2] \tag{8}$$

$$E_\theta = k_{ijkl} \sum_{n=0}^{m} C_n \cos(n\theta) \tag{9}$$

$$E_\omega = k_{ijkl}[C_0 + C_1 \cos(\omega_{ijkl}) + C_2 \cos(2\omega_{ijkl})] \tag{10}$$

$$E_\phi = k_{ijkl} \sum_{n=0}^{m} C_n \cos(n\phi_{ijkl}) \tag{11}$$

The energy of non-bond interaction is generally accounted for: the Van der Waals interactions (E_{vdw}) and the electrostatic interactions (E_{el})

$$E_{nonbond} = E_{vdw} + E_{el} \tag{12}$$

$$E_{vdw} = D_{ij}\{-2[\frac{x_{ij}}{x}]^6 + [\frac{x_{ij}}{x}]^{12}\} \tag{13}$$

$$E_{el} = 332.0637(\frac{Q_i Q_j}{\varepsilon r_{ij}}) \tag{14}$$

The Van der Waals interactions (E_{vdw}) (13) are connected with Lennard-Jones potential, where D_{ij} is the potential well depth and x_{ij} is the sum of Van der Waals radii. The electrostatic interactions (E_{el}) (14) are described by the atomic monopoles and a screened (distance-dependent) Coulombic term, where Q is the electric quantity and ε is the dielectric constant.

The force field parameters needed for the dynamic simulation of ion adsorption on the $Mg(OH)_2$ planes were provided by the parameter generator which exists in

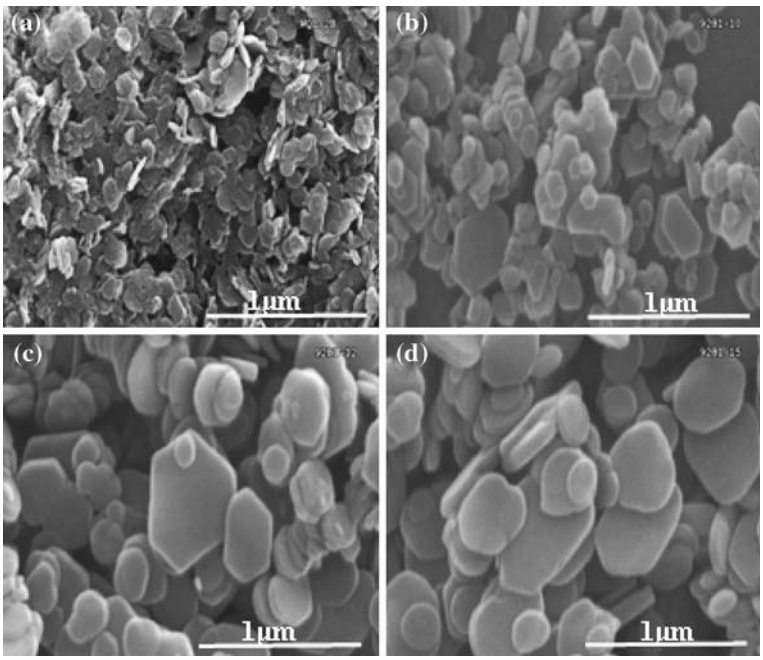

Fig. 1 Influence of $CaCl_2$ on the morphology of $Mg(OH)_2$. Initial concentration of $CaCl_2$ (g/L): a-0(without hydrothermal modification), b-0, c-1.5., d-3.0; Temperature (°C): 200, time (h): 4.0

Table 1 Influence of $CaCl_2$ on the average size of $Mg(OH)_2$ (Temperature: 200 °C, time: 4.0 h)

Concentration g/L	Diameter size μm	Thickness μm	Ratio of diameter to thickness
0.0	0.3	0.02	15
1.5	0.5	0.02	25
3.0	0.75	0.03	25

Universal force field and can calculate the forcefield parameters by combining the atomic parameters.

Results and discussion

Hydrothermal modification of $Mg(OH)_2$ in $CaCl_2$ solution

Figure 1 shows the morphologies of $Mg(OH)_2$ before and after hydrothermal modification at 200 °C for 4.0 h in the aqueous solutions containing different amount of $CaCl_2$. Irregular fine plates with a diameter of about 0.1–0.2 μm were formed at room temperature (Fig. 1a). The influence of $CaCl_2$ on the average size of $Mg(OH)_2$ was shown in Table 1. The diameter of the plates increased slightly to 0.3 μm and the thickness was 0.02 μm after hydrothermal treatment in water (Fig. 1b). The addition of minor amount of $CaCl_2$ in the hydrothermal solution enlarged the particle size of $Mg(OH)_2$ obviously. The diameter size was 0.5 μm at 1.5 g/L $CaCl_2$ (Fig. 1c) and increased up to 0.75 μm in the cases of 3.0 g/L $CaCl_2$ (Fig. 1d), while the change of thickness was not obvious (about 0.02 μm in the case of 1.5 g/L $CaCl_2$ and 0.03 μm in the case of 3.0 g/L $CaCl_2$). The ratio of diameter to thickness increased when the concentration of $CaCl_2$ increased from 0 to 3.0 g/L.

XRD patterns of the samples were shown in Fig. 2. For the precipitates formed at room temperature, the peak strength of the (101) plane was stronger than that of the (001) plane. The strength of (001) plane became stronger than that of (101) plane after hydrothermal treatment and this tendency became more obvious at higher $CaCl_2$ concentration. Further analysis of the XRD data indicated that the cell parameters of the modified $Mg(OH)_2$ increased slightly with the increase of $CaCl_2$ concentration. The cell parameters of $Mg(OH)_2$ increased to a = 3.147 Å, c = 4.768 Å in the presence of 1.0 g/L $CaCl_2$, which may be connected with the intercalation of Ca^{2+} in $Mg(OH)_2$ crystals. Chemical analysis confirmed that the content of Ca in $Mg(OH)_2$ increased from 0 in the absence of $CaCl_2$ to 0.72 wt.% in the presence of 1.0 g/L $CaCl_2$.

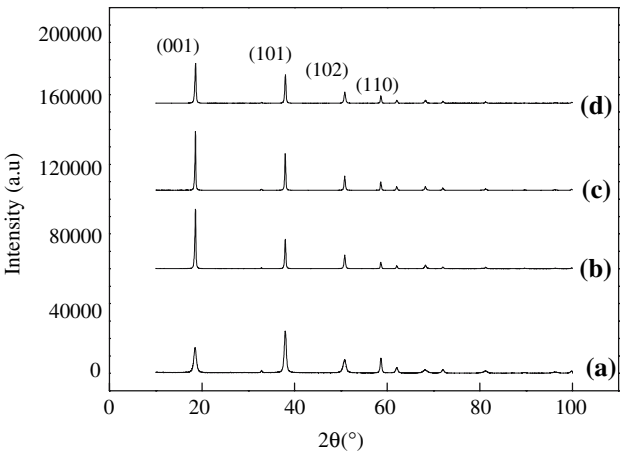

Fig. 2 Influence of $CaCl_2$ on the XRD patterns of $Mg(OH)_2$. Initial concentration of $CaCl_2$ (g/L): a-0 (without hydrothermal modification), b-0, c-1.0, d-3.0; temperature (°C): 200, time (h): 4.0

Theoretical simulation of $Mg(OH)_2$ morphology

$Mg(OH)_2$ belongs to the layered CdI_2-type (space group $P\bar{3}ml$) structure, with a = b = 3.0698 Å, c = 4.429 Å and $\alpha = \beta = 90$, $\gamma = 120$ [20]. Successive hexagonal Mg^{2+} layers and OH^- layers are stacked one upon another, which is favorable for the formation of the platelet crystals. There is a slight expansion of the cell parameters to a = b = 3.1021 Å, c = 4.7009 Å, after the geometry optimization using Smart algorithm and Universal Force Field, resulting in an increase of the cell volume up to 8.38%. The equilibrium morphology of $Mg(OH)_2$ (Fig. 3) was estimated using the Morphology package.

Figure 4 shows that the polyhedral shape was the equilibrium morphology of $Mg(OH)_2$. (001) and (00$\bar{1}$) planes were vertical to the *Z* axis. There are 12 main planes parallel to the *Z* axis, including (100), ($\bar{1}$00), (010), (0$\bar{1}$0), ($\bar{1}$10), (1$\bar{1}$0), (110), ($\bar{1}\bar{1}$0), (2$\bar{1}$0), ($\bar{2}$10), (1$\bar{2}$0) and ($\bar{1}$20). According to the symmetry of the $Mg(OH)_2$ crystal, these planes can be divided into three groups: (001) and (00$\bar{1}$); (100), ($\bar{1}$00), (010), (0$\bar{1}$0), ($\bar{1}$10) and (1$\bar{1}$0); (110), ($\bar{1}\bar{1}$0), (2$\bar{1}$0), ($\bar{2}$10), (1$\bar{2}$0) and ($\bar{1}$20).The planes in each group have the same atomic arrange and structure. (101) surface

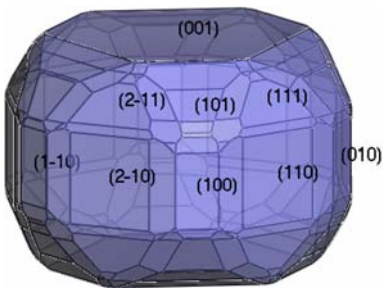

Fig. 3 The equilibrium morphology of $Mg(OH)_2$ crystal

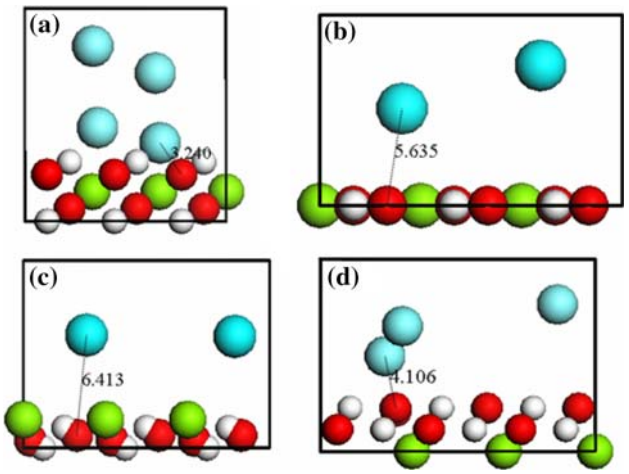

Fig. 4 Adsorption configuration of Ca^{2+} on $Mg(OH)_2$ planes. (**a**) (001), (**b**) (110), (**c**) (101), (**d**) (100); : Mg, : O, : H, : Ca

is a diagonal plane which expressed in the morphology. Four planes with low Miller index, (001), (100), (110) and (101), were chosen to simulate the adsorption behavior of Ca^{2+} and Cl^- since these planes are comparatively stable owing to their smaller inter-planar distances.

Adsorption of Ca^{2+} and Cl^- on $Mg(OH)_2$ planes

(001), (100), (110) and (101) planes were originated from the geometry optimization cell and enlarged to 3 × 3 super-planes. The 2-D super-planes were converted to 3-D planes with a magnitude of 10 Å vacuum upon the plane. The adsorption of Ca^{2+} and Cl^- on (001), (101), (110) and (100) planes were estimated at 473 K and 1.5 MPa. Ca^{2+} and Cl^- can change their position and orientation in the framework. The simulation time was 1,000,000 time steps of 1.0 fs. Table 2 listed the capacity and the energy for the adsorption of Ca^{2+} and Cl^-. The negative adsorption energies indicated that it is energetically favorable for the adsorption of Ca^{2+} and Cl^- on the $Mg(OH)_2$ planes.

The lower energy (–0.435 kJ/mol) and higher adsorption capacity (0.491 molecules per cell) for the adsorption of Ca^{2+} on (001) plane than on other planes indicated the easier adsorption of Ca^{2+} on (001) plane. The adsorption order for Ca^{2+} and Cl^- were (001) > (100) > (101) > (110) and (101) > (100) > (001) > (110) respectively, according the corresponding loading and energy values. Adsorbed ions would inhibit the growth of a plane by incorporating into the plane. From the $Mg(OH)_2$ cell structure, we calculated the maximum radius of ions that can inhabit in the $Mg(OH)_2$ plane is 1.535 Å. The radius of OH^- is 1.36 Å while that of Cl^- is 1.81 Å. The radius of Ca^{2+} is 0.99 Å, which is a little bigger than that of Mg^{2+} 0.66 Å. So the influence of Ca^{2+} on the growth of $Mg(OH)_2$ should be much obvious than that of Cl^- since the substitution of OH^- by Cl^- was quite difficult due to their big difference in ion radius [21–22].

Figure 4 show the adsorption configuration of Ca^{2+} on $Mg(OH)_2$ planes based on the principle of the minimum adsorption energy. The distance between the adsorbed Ca^{2+} and the oxygen atom in (001) plane is 3.240 Å, quite similar with the distance between magnesium and oxygen atoms (3.115 Å) in (001) plane, indicating the possible incorporation of Ca^{2+} on the (001) plane. The adsorption of Ca^{2+} on (100), (110) and (101) planes were difficult since the distance between Ca^{2+} and O^{2-} in these planes are 4.106 Å, 5.635 Å, and 6.413 Å, respectively, which exceed the available interaction distance (2–4 Å) [23]. It was induced that the adsorption of Ca^{2+} on (001) plane may decrease the growth rate of (001) plane while the growth of (101) and (110) planes was little influenced by the existence of Ca^{2+}, leading to the decrease of the aspect ratio of the $Mg(OH)_2$ plates, the occurrence of the remain plane (001) and the gradual disappearance of (101) and (110) planes.

Conclusion

The atomistic dynamics simulation method was used to study the hydrothermal adsorption of $CaCl_2$ on $Mg(OH)_2$ planes. The adsorption behavior of Ca^{2+} and Cl^- ions were estimated based on the corresponding absorption energies and capacities on (001), (101), (110) and (100) planes of $Mg(OH)_2$ at elevated temperature. The simulation results indicated that it was easier for Ca^{2+} to be adsorbed on the (001) plane than on the other planes due to the lower adsorption energy and the higher capacity. The adsorption of Ca^{2+} on (001) plane at elevated temperature may inhibit the growth of the (001) plane, leading to occurrence of the (001) plane, the shrinkage of the (101) and (110) planes

Table 2 Capacity and energy for the adsorption of Ca^{2+} and Cl^- on $Mg(OH)_2$ planes

Sorbate plane	Ca^{2+}				Cl^-			
	(001)	(101)	(100)	(110)	(001)	(101)	(100)	(110)
Capacity/molecules per cell	0.491	0.266	0.367	0.238	0.265	0.466	0.356	0.258
Energy/kcal mol^{-1}	–0.435	–0.318	–0.423	–0.259	–0.398	–0.511	–0.507	–0.322

and the formation of $Mg(OH)_2$ plates with bigger ratios of diameter to thickness.

References

1. Donnay JDH, Harker D (1937) Am Mineral 22:463
2. Hartman P, Perdok WG (1955) Acta Cryst 8:49
3. Grimbergen RFP, Meekes H, Bennerma P (1999) Acta Cryst A55:84
4. Nassralla AN, Boughriet A, Fischer JC, Wartel M (1996) A J Chem Soc, Faraday Trans 92:3211
5. Yang DN, Wang RM, Liu ZF (2004) Nanotechnology 15:1625
6. Trnrikulu SU, Eroglu I, Bulutcu AN (1998) J Cryst Growth 194:220
7. Leeuw NH (2002) J Phys Chem B 106:5241
8. Rothon RN (2000) Magnesium hydroxide: new products, processes and applications. In: Intertech, 19 Northbrook Drive, Portland, Maine (Ed.), Functional Effect Filler. Berlin, Germany
9. Rothon RN, Carus D, Elsner D (1999) Chem Aust (Jan–Feb) 35
10. Lv JP, Qiu LZ, Qu BJ (2004) J Cryst Growth 267:676
11. Li YD, Sui M, Ding Y, Zhang G H, Jing Z, Wang C (2000) Adv Mater 12:11
12. Phillips VA (1977) J Cryst Growth 41:228
13. Phillips VA (1977) J Cryst Growth 41:235
14. Henrist C, Mathieu JP, Vogels C, Rulmont A, Cloots R (2003) J Cryst Growth 249:321
15. Materials Studio 4.0, Sorption (2005) Accelrys Company, USA
16. Frenkel D, Smit B (2002) Understanding molecular simulation: from algorithms to applications, 2nd edn. Academic Press, San Diego
17. Wulff G (1901) Z Krist 34:449
18. Rappe AK, Casewit CJ, Colwell KS (1992) J Am Chem Soc 114:10024
19. Casewit CJ, Colwell KS (1992) J Am Chem Soc 114:10035
20. Chakoumakos BC, Loong CK, Schltz AJ (1997) J Phys Chem B 101:9458
21. Dharmasena G, Frech R (1993) J Chem Phys 99:8929
22. Wu QL, Xiang L, Jin Y (2006) Powder Technol 165:100
23. Cooper TG, Leeuw NH (2003) Surf Sci 531:159